

THE OFFICIAL MAGAZINE OF THE OCEANOGRAPHY SOCIETY

Oceanography

CITATION

Mullarney, J.C., S.M. Henderson, B.K. Norris, K.R. Bryan, A.T. Fricke, D.R. Sandwell, and D.P. Culling. 2017. A question of scale: How turbulence around aerial roots shapes the seabed morphology in mangrove forests of the Mekong Delta. *Oceanography* 30(3):34–47, <https://doi.org/10.5670/oceanog.2017.312>.

DOI

<https://doi.org/10.5670/oceanog.2017.312>

COPYRIGHT

This article has been published in *Oceanography*, Volume 30, Number 3, a quarterly journal of The Oceanography Society. Copyright 2017 by The Oceanography Society. All rights reserved.

USAGE

Permission is granted to copy this article for use in teaching and research. Republication, systematic reproduction, or collective redistribution of any portion of this article by photocopy machine, reposting, or other means is permitted only with the approval of The Oceanography Society. Send all correspondence to: info@tos.org or The Oceanography Society, PO Box 1931, Rockville, MD 20849-1931, USA.

A Question of Scale

How Turbulence Around Aerial Roots Shapes the Seabed Morphology in Mangrove Forests of the Mekong Delta

By Julia C. Mullarney, Stephen M. Henderson, Benjamin K. Norris, Karin R. Bryan,
Aaron T. Fricke, Dean R. Sandwell, and Daniel P. Culling

Background photo. Aerial root structures (pneumatophores) protrude from the seabed in this photograph of the fringe from a mangrove forest in the Mekong Delta.

ABSTRACT. Mangrove forests are highly productive ecosystems that provide many physical, societal, and ecological services in tropical and subtropical regions. Accurate prediction of the morphological evolution for these areas, in the face of global sea level rise and changes in sediment supply, requires understanding of interactions between vegetation growth, water flows, and sediment transport. Data presented from a wave-exposed mangrove forest in the Mekong Delta, Vietnam, include unique measurements that resolved water flows in and around the aerial mangrove roots (known as pneumatophores) over scales from a few millimeters to hundreds of meters. Flows were highly turbulent, with turbulence values sometimes as large as those measured in surf zones. These energetic processes appear to stir up sediments, with small scour troughs observed around individual pneumatophores, and larger-scale scour around clusters of pneumatophores. The vegetation fringe (the boundary between forest and mudflat) was a particularly dynamic area, with elevated turbulence levels, greater vegetation densities, coarser sediments, and occasional wave breaking. Intense turbulent dissipation at the fringe then reduces the energy of shoreward-propagating waves, sheltering the forest interior. The small-scale processes appear to be linked with forest-wide patterns of sediment transport and deposition. We discuss these links in the context of the biophysical interactions that control the changing shapes of deltas worldwide.

INTRODUCTION

As the Mekong River approaches Vietnam's East Sea (South China Sea), the river channel becomes less steep, the river waters lose their carrying capacity, and sediments are deposited to form the Mekong Delta. Over geological time, much of the land that is now southern Vietnam was created in this manner, although present land-building processes may be changing due to dam construction, sediment mining, removal of marshes, construction of dikes, and sea level rise (Allison et al., 2017, and Liu et al., 2017, both in this issue).

Changing marine conditions and the flow of the Mekong River, which rises and falls each year with the monsoon cycle, continually reshape the delta. The marine processes at work include the action of waves, tides, and storm surges, which erode and deposit sediments. The many aquatic plants that naturally populate delta shorelines further influence development of the coastline. Particularly notable are intertidal forests of *Sonneratia caseolaris*, mangrove trees that can grow to over 10 m in height. The stems, branches, roots, and leaves of aquatic vegetation act as obstacles to water flow,

adding a biological dimension to the already-complex interactions between hydrodynamics and sediment movement within deltaic regions. Mangrove trees, in particular, are surrounded by intricate aerial root systems that control gas (oxygen) exchange and salt filtration, allowing these plants to tolerate submersion in saline water and to grow in oxygen-poor sediments. Across the wide variety of mangrove species, aerial roots are found in many different shapes and sizes, including “stilt,” “knee,” and “pencil” forms. The pencil pneumatophore roots are predominantly associated with the *Sonneratia* and *Avicennia* tree species. Pneumatophores protrude a few tens of centimeters above the seabed, growing upward from the underground lateral roots, which extend from the central tree trunk to form a radial, spoke-like pattern. Often, tens or hundreds of 1 cm diam r roots are found per square meter of bed. In the present work, we refer to the collection of pneumatophore roots as a “canopy.” This term is a common way of referring to underwater vegetation, arising from the similarity to a forest canopy influencing the wind.

Pneumatophores and tree trunks

enhance the frictional effect (drag) of the vegetation on the water column. During flooding tides, there is a sudden change in drag as currents enter a mangrove forest from offshore tidal flats (Mazda et al., 1997). The vegetation slows the flow and causes the water surface to tilt. In the case of tidal currents flowing along the forest boundary, the frictional effect can cause the currents to rotate into the forest in a manner resembling the rotation of groundwater as it moves across a boundary from high to low hydraulic conductivity in aquifers (Bear, 1979). On a smaller scale, pneumatophores generate stem-scale turbulence through the processes of vortex shedding and eddy generation (Figure 1). Larger-scale tidal and wave energy is thus converted into dissipative wake-scale turbulence (Norris et al., in press). As energy is extracted from the flow, turbulent mixing is likely enhanced, and the stresses acting at the seabed are altered. Turbulent mixing plays an important role in controlling the vertical distribution of sediments through the water column, while bed stress likely controls the balance between sediment resuspension and deposition at the bed. On some vegetated shorelines, low-flow zones are created that prevent sediment resuspension and allow deposition to occur (e.g., as in salt marshes observed by Pratolongo et al., 2010). However, vegetation does not always enhance deposition, and may actually encourage erosion (Bouma et al., 2007; Nardin and Edmonds, 2014; Tinoco and Coco, 2016). Given current knowledge, predicting in advance whether vegetation will encourage erosion or deposition at a given location can be difficult. One impediment to development of improved understanding is the scarcity of turbulence measurements within vegetation canopies, which leaves many models for within-canopy mixing and bed stress poorly constrained (Le Bouteiller and Venditti, 2015). At great stem densities, the shear (canopy) turbulence that is

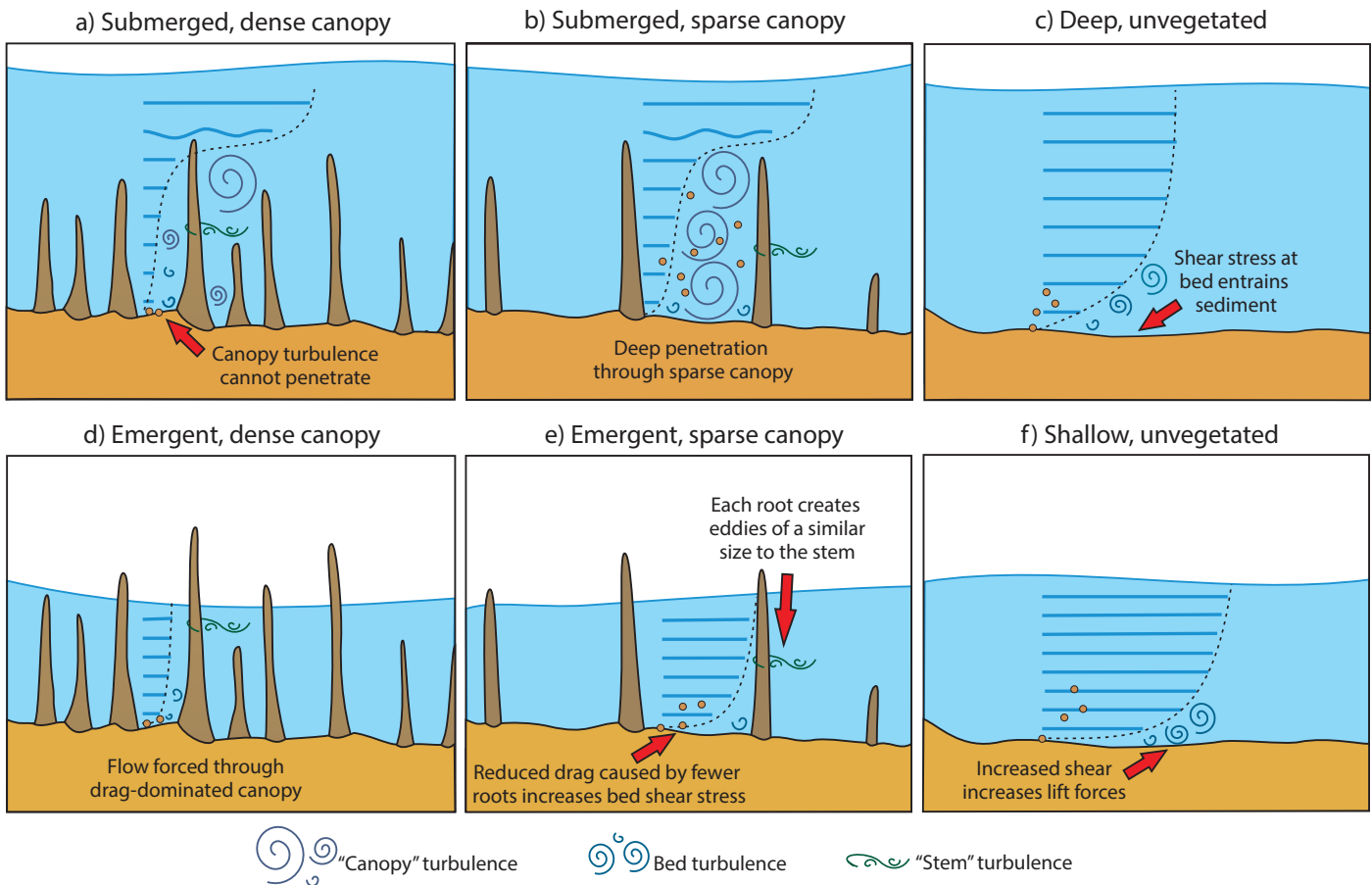


FIGURE 1. Turbulent processes and velocity profiles within pneumatophore (root) “canopies” (a,b,d,e) and above an unvegetated bed (c and f). Note that “stem” scale is used to describe turbulence generated from the pneumatophores to strengthen the analogy with other vegetation types such as salt marsh plants.

generated at the canopy/water interface cannot penetrate downward to reach the bed (Figure 1a,d). Conversely, for lesser vegetation densities, shear stress can reach the bed, enhancing resuspension of sediments (Figure 1b,e).

In recent years, substantial progress has been made in the area of the interaction between vegetation and flow, at both small (Nepf, 2012a,b) and large scales (Fagherazzi et al., 2012; Coco et al., 2013; Nardin et al., 2016a). At the small scale, work has been conducted in laboratory flumes using mimics or plants with approximately uniform or simplified morphologies. However, natural vegetation often has rough surfaces (such as the barnacles and bark naturally present on pneumatophores) and is highly variable. Even within a single forest or marsh, there can exist considerable heterogeneity of vegetation characteristics (e.g., density, stiffness, length), bathymetry, and hydrodynamic forces. Moreover, both plant

growth and environmental conditions vary with seasons, and in order to predict longer-term evolution, the strong ecogeomorphological feedbacks must be parameterized (van Maanen et al., 2015). Such conditions contribute to the inherent complexity of these regions (Mullarney and Henderson, in press).

The physical and biophysical processes within deltas and mangrove forests are also modulated by anthropogenic activities. Many deltas worldwide (including the Mekong) support large human populations, but are sinking due to sea level rise; compaction from water, oil, gas, and sand removal; and dam building that affects sediment supply (Syvitski et al., 2009; Anthony et al., 2015). It is not yet clear how recently reported changes in Mekong sediment supply (Nowacki et al., 2015; Darby et al., 2016) may contribute to the alteration of this landscape.

To date, a complete understanding of how the small-scale processes contribute

to and shape the large-scale processes is lacking. Indeed, even the appropriate scale over which to measure is still an open question. Additionally, in situ measurements are often limited, partly because many mangrove forests are in remote and difficult-to-access areas. However, the local processes of sediment erosion and deposition, combined with sediment supply and transport between regions of mangrove forests, need to be understood. The subsequent expansion of these processes may be critical to delta-scale evolution (Fagherazzi et al., 2017, in this issue; Bryan et al., in press).

We collected data from a mangrove forest in the Mekong Delta to explore the complex interactions between vegetation, sediment transport, and hydrodynamics, considering both small-scale turbulence and larger-scale wave and tidal motions. Measurements were collected near the wave-exposed seaward fringe (i.e., the boundary between mudflat

and forest) of a mangrove forest on the island of Cu Lao Dung, in the Soc Trang Province, Vietnam. The fringe region of the forest is predominantly composed of *Sonneratia caseolaris* trees (Bullock et al., in press), with *Avicennia* and *Aegiceras corinculatum* mangroves and *Nypa fruticans* palms within the forest interior (Hong and San, 1993). This field site provides an intriguing location for a study because, despite limited physical separation (~12 km), the two different sides of the island form distinct and contrasting environments. The southwest side of the forest is characterized by a more coarse-grained substrate, and is prograding rapidly (average rate of seaward progradation since 1970 is ~60 m yr⁻¹; Fricke et al., in press). On the northeast side, the substrate is more fine grained, the forest is narrow and more mature, and the area has been subjected to erosion since 2009 (Nardin et al., 2016b). Moreover, the island is subject to seasonal northeast and southwest monsoons, which provide a range of climatic conditions, including exposure to waves from the Vietnam's East Sea and variations in the discharge from the Mekong River.

Our observations focus on small-scale hydrodynamic measurements, together with characterization of surface sediments and vegetation densities. These observations raise questions relevant to broader-scale delta morphodynamics. In particular, we consider the role of vegetation in encouraging deposition in some cases, but erosion in other cases. Our case study will provide insight not only into the evolution of the Mekong Delta but also, by extension, into the sediment-transport processes that govern the changing shapes of tropical deltas worldwide.

FIELD EXPERIMENTS

Scientists from five universities in Vietnam, the United States, and New Zealand measured water flows, characterized sediment deposits, and mapped vegetation patterns within and immediately offshore of the mangroves on the seaward fringe of Cu Lao Dung. This

international collaboration between multiple institutes, coupled with riverine, shelf, remote-sensing, and modeling studies (see Nittrouer et al., 2017, in this issue), provided an exciting opportunity to obtain a comprehensive set of measurements over a range of scales. Experiments were conducted in September 2014 and March 2015, with each experiment lasting approximately two weeks. During September (the southwest monsoon), wind speeds were slow, wave heights relatively small, and river discharge was high. March represented the comparatively drier northeast monsoonal conditions, with stronger winds, larger waves, and lower river discharge.

Hydrodynamic Measurements

Our observations at each side of the island focused on a roughly fringe-perpendicular transect, with instrument deployments extending 150 m onshore and offshore of the forest edge to capture the flow transitions and sediment changes over the varying substrates and regions of different vegetation. Each deployment location was classified as one of the three major environment types: mudflat, fringe, or forest. The experiments used a combination of fixed instruments that remained in the same location throughout the experiment and movable arrays that were left in situ for multiple tides before relocation (Figure 2).

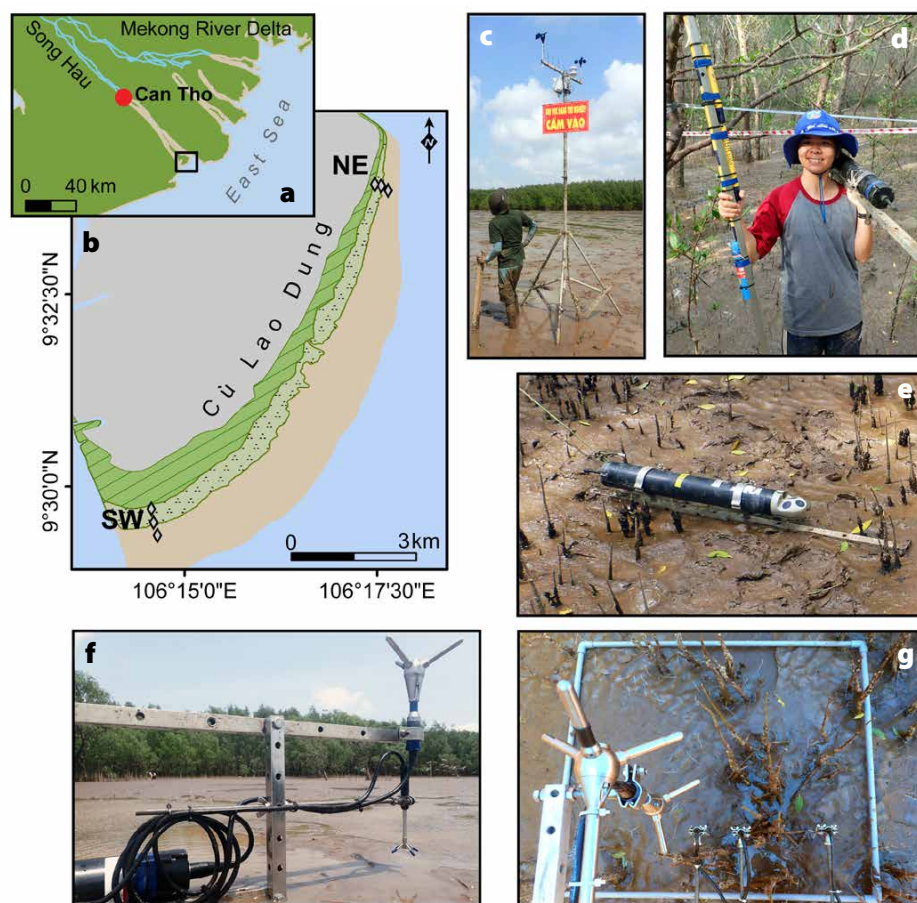


FIGURE 2. (a) Location of Cu Lao Dung on the Mekong River Delta. (b) Approximate deployment locations across the three different environments (forest, fringe, and mudflat). Brown is mudflat, light green with dots shows forest dominated by *Sonneratia* species, and the dark green shows the area mostly inhabited by *Avicennia* and *N. fruticans*. The distinction between dominant mangrove types was digitized from Google Earth and from data sets provided by Bullock et al. (in press). (c) to (g) Instrumentation was used in multiple configurations during the field experiments: (c) weather station on mudflat, (d) temperature probes, (e) acoustic Doppler current profiler, and (f and g) acoustic Doppler velocimeters. The larger instruments provide single point measurements, and the smaller instruments are Vectrino Profilers that provide high-resolution (temporal and spatial) profiles of velocity.

Flow speeds and directions were measured using a variety of acoustic current meters. During longer-term deployments, acoustic Doppler current profilers (ADCPs) generally measured profiles of water velocity, sampled every 100 mm throughout the entire water column (sampling at 2 Hz and averaged over 2 minutes every 10 minutes to reduce noise). For short-duration movable-array deployments, ADCPs were often configured in pulse-coherent mode, which provides profiles of currents with better resolution in the vertical (typical cell sizes were 25 mm) and a faster sampling rate (usually 8 Hz). For our deployments, vertical profile lengths were between 0.2 m and 0.45 m. Point measurements of velocity were also recorded at 32 Hz by acoustic Doppler velocimeters (ADV). Additional instrumentation included pressure sensors and conductivity-temperature-depth (CTD) sensors. To measure small tide-induced lateral pressure gradients, horizontally displaced depth sensors were placed in thermally insulated flasks with small openings to minimize temperature-dependent errors in the pressure readings. These flasks were buried beneath a couple of centimeters of sand to minimize Bernoulli effects (such effects would influence pressure measurements if flows were disturbed by the presence of the instruments). A weather station was deployed to measure winds and atmospheric pressure 3.6 m above the mud flats, 130 m from the forest edge, on the southwest side of the island.

A novel feature of these experiments was the use of three Nortek Vectrino Profilers. Designed for laboratory use, these profilers required a power supply and cabled logging directly to a laptop (see Box 1). Although the arrangement created logistical challenges in the hostile field environment, the advantage was that these instruments capture velocity profiles at very high temporal (up to 100 Hz) and spatial resolution (measurements every 1 mm along a 35 mm profile). The Vectrino Profilers were deployed in a range of configurations on the flats and

in the forest, both within and above the pneumatophore canopy, and at varying proximities to pneumatophores.

Although generally of a high quality, data underwent evaluation to remove, for example, velocity spikes and low-correlation data. The dissipation rate of turbulent kinetic energy, ϵ , was estimated using the structure-function method (Wiles et al., 2006). Accordingly, turbulence characteristics are extracted by measuring how the velocities decorrelate along each acoustic beam. This technique allows the separation of currents caused by turbulence from the oscillatory currents caused by waves, which decorrelate over a much larger scale. This method has been successfully employed to estimate turbulence in rivers (MacDonald and Mullarney, 2015), in highly turbulent swash zones (Lanckriet et al. 2013), and in mangroves (Norris et al., in press). The dissipation rate, with units $W\ kg^{-1}$, is the rate for loss of turbulent kinetic energy through viscosity to heat, and it is commonly used as a measure to characterize turbulence. Values range over many orders of magnitude, from $10^{-10}\ W\ kg^{-1}$ in the abyssal ocean and stratified lakes to $10^{-1}\ W\ kg^{-1}$ in highly energetic regions such as some narrow tidal straits and the most energetic of surf and swash zones (e.g., Thorpe, 2005).

Vegetation Measurements

Detailed bathymetric surveying plays a vital role in the conventional modeling of estuaries. High-resolution bathymetry is often required to obtain good model skill, and much effort has been devoted to development of technologies such as multibeam sonar to provide the required data. When simulating flow through vegetation, measurements of vegetation geometry play a similar role, because model predictions depend fundamentally on the type of canopy through which water flows. However, technologies for resolving the complex geometry of natural canopies have often been very limited, and many studies have depended on old-fashioned hand measurements using

rulers, calipers, and pencil and paper. In our study, we used recently developed photogrammetric techniques to better resolve the three-dimensional structure of the numerous stems that compose natural pneumatophore canopies. At each instrument deployment site, vegetation characteristics were surveyed within a $1\ m^2$ quadrat using the method of Liénard et al. (2016). This technique involves taking numerous (~ 200) photographs of the quadrat from multiple viewpoints, then reconstructing a dense three-dimensional point cloud using overlapping features recognized within multiple photographs (Figure 3). A computer algorithm (“sector slice”) is then used to identify the set of points corresponding to the location of each pneumatophore stem, and stem diameters are determined for heights extending from within 1 cm of the bed every 5 mm to the top of the canopy. From this method, the location and number of stems is produced with associated vegetation geometries for each height “slice.”

Relative to conventional hand measurements, this method has several advantages: a profile of properties is obtained over the entire depth of the canopy at a much improved resolution, and the position of instruments relative to every pneumatophore can be more easily determined. Furthermore, field sampling with this method is relatively rapid, with each photo survey completed in about 5 to 10 minutes, plus 30 minutes of image processing, compared to tens of minutes, or even hours, required for traditional methods. Measurements were collected every 5 mm along a vertical profile to provide a variety of key summary statistics, especially the proportion of total canopy volume occupied by solid stems, denoted $\phi(z)$, and the frontal-area density with height above the bed, denoted $a(z)$ (i.e., the cross-sectional area of stems, normal to the water-flow direction, per unit volume of canopy [units m^{-1}]). The statistic a is particularly important for hydrodynamic models because it often appears in parameterizations for canopy drag.

Box 1. Instrumentation Challenges: From the Laboratory to the Field

A key feature of our instrument array was the deployment of three synchronized Nortek Vectrino Profilers, which enabled fast measurements (up to 100 Hz) at millimeter scales. These instruments are primarily designed for laboratory measurements, so some creativity was required to use them in the field (Figure B1). Additionally, the remote study site in the Mekong Delta, Vietnam, demanded simplicity and redundancy.

The Vectrino is supplied with an AC/DC voltage transformer outputting 24 VDC and requires a PC for configuration, data display, and logging (via RS-422 communication cable). To avoid the safety risks and low efficiency associated with powering the Vectrinos and PC using a battery and inverter, we powered the system using two moped 12 VDC sealed lead-acid or valve-regulated lead-acid (SLA or VRLA) batteries (of 9–12 amp hours), wired in series, and blade fuses. The battery cell connected directly to the supplied Vectrino cable. These batteries and fuses are readily available in Vietnam. A single 12 V battery would power the Vectrino in the field, although the instrument would disconnect once power dropped below 12 V, thus missing out on 25% of the battery's charge. Bench tests in the laboratory before departure yielded the recommended fuse rating (between 0.9 amps and 1.095 amps). This system provided power sufficient for 7 to 10 hours of run time.

The power and communication systems required waterproofing for field deployment. The power pack (2 × 12 VDC SLA batteries, fuse holder, fuse) was housed in a waterproof case with IP68 cable glands. The power cables from the power box and the Vectrino communication cables (RS-422, USB converter) were all housed in an outdoor waterproof electrical box (hereafter referred to as comms. box) with silicon blocks that clamp on the cables when the lid is closed to provide seal. The USB communication cables from the comms. box were connected to a laptop housed in a waterproof cover. An additional power supply was constructed in a waterproof case using a 150 W laptop power supply wired directly to a 12 VDC SLA battery that provided an additional three hours of laptop use (Figure B2a).

One-hundred-meter RS-422 communication cables were used to distribute Vectrinos spatially from a central station (e.g., our inflatable kayaks, a Vietnamese fishing boat, and our bamboo tree platform; Figure B2). These 100 m cables can be challenging to keep tidy, but a PVC pipe arrangement provided a simple solution for organization. The three Vectrinos were synchronized by connecting all the Sync+ lines together and all the Sync- lines together. Data were collected at a sampling rate of 50 Hz (baud rate 937500) and saved in 10-minute files.

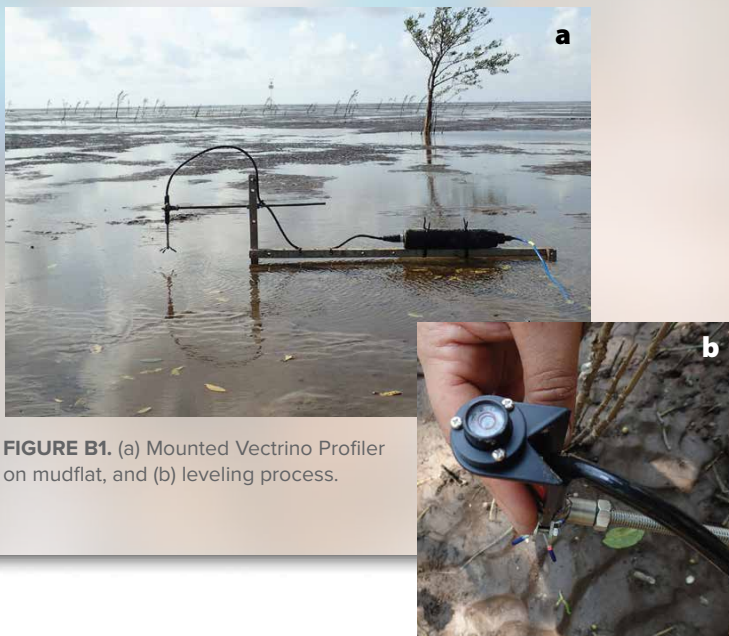


FIGURE B1. (a) Mounted Vectrino Profiler on mudflat, and (b) leveling process.



FIGURE B2. Power and instrumentation set up on (a) kayaks, (b) a Vietnamese fishing boat, and (c) a bamboo tree platform. The cable organizers are located on the blue kayak, and the orange kayak carries the power supply, communications box, and laptop.

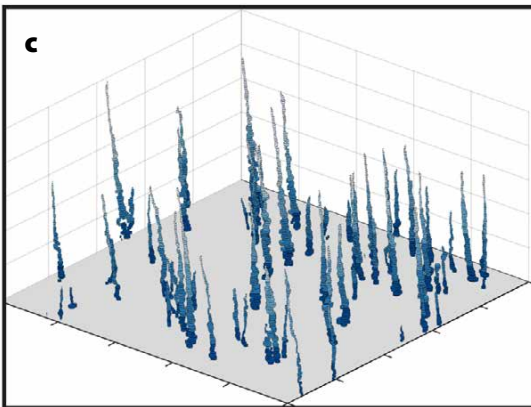
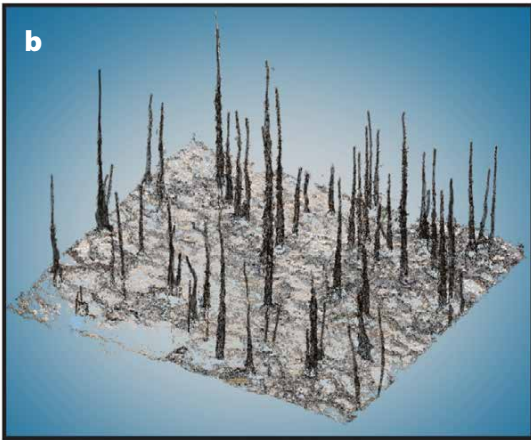


FIGURE 3. Illustration of the photogrammetric technique used to obtain high-resolution estimates of pneumatophore geometries. (a) Example photograph showing a 1 m² quadrat placed around pneumatophores and acoustic instruments. (b) Photogrammetric reconstruction of the dense point cloud (after removal of instruments). (c) Pneumatophores represented as three-dimensional shapes with individual circular cylinders at each horizontal cross-section elevation and location, fitted to the three-dimensional point cloud. Cylinder diameters are twice the mean of the radius for each slice as generated by the sector-slice algorithm (Liénard et al., 2016).

Sediment Measurements

Grab samples, hand samples, and sediment cores were collected to examine both changes in sediment character over short time scales (between seasons) and rates of sediment accumulation over longer time scales (decadal to centennial) across the differing mudflat, fringe, and forest environments. Sediment grain size was determined by separating the sand and mud fractions of each sample by wet sieving through a 64 μm sieve, and then further analyzing the mud fraction using laboratory particle sizers. To provide a snapshot of present-day sediment transport, time series of suspended sediment concentrations were obtained from optical backscatter sensors (OBS), which were calibrated using in situ water samples. In general, these sensors were co-located with current profilers. Measurements were collected for 6 to 8 minutes every 10 minutes at either 2 Hz or 6 Hz.

A VARIED AND CHANGEABLE ENVIRONMENT: DIFFERENCES ACROSS MULTIPLE SCALES

Mudflat-to-Forest Spatial Scale and Seasonal Time Scale

During both seasons, there was a strong alongshore component of flow on both sides of the island (toward the west on the southwest side and toward the north on the northeast side), likely driven by the larger-scale tidal and riverine dynamics. This alongshore component of flow was further enhanced on the southwest side by strong alongshore winds (wind speeds were not measured on the northeast side). Flow speeds on the southwest reached up to 0.62 m s⁻¹ on the mudflat, whereas velocities were generally smaller on the more steeply sloping northeast side. Waves were often a major contributor to the total water velocity and, as with flow speeds, wave heights were larger on the southwest side, with maximum significant wave heights on the mudflat just outside of the fringe reaching 0.33 m in September and 0.67 m in March, compared to 0.26 m and 0.51 m on the northeast side, respectively (Figure 4e,f).

On entering the forest, the alongshore component of tidal velocities rapidly declined, indicating a marked flow rotation to a direction that is approximately perpendicular to the vegetation fringe. Changes in friction drove the rotation, with drag coefficients over the whole area estimated to be 10 to 30 times larger in the forest than on the mudflat (Mullarney et al., in press). Such patterns were observed during both seasons and reflect the influence of vegetation on both the small-scale (flow between root canopies) and large-scale (system-wide wave and tidal energy damping) flow regimes. These flow patterns are comparable to those observed in different mangrove systems: flow rotation was seen in a sheltered and channelized mangrove system in Thailand (Horstman et al., 2013, 2015), and Chen et al. (2016) reported a similar flow rotation for a forest in China populated by young *Kandelia obovata* and *Aegiceras corniculatum* trees. In this latter system, trees had a mean height of 1.6 m and did not have a well-developed emergent root system. Hence, the tree trunks, branches, and leaves were the main suppliers of friction.

Time series of velocities from instruments that were closely spaced within the fringe region suggest that flows are highly variable over 10 m scales (Bryan et al., in press). In particular, for the initial stages of the flooding tide (water heights <0.5 m), local bathymetric changes such as small runnels, bedforms, and scour around patchy vegetation appeared to have a large influence and introduced considerable alongshore variability to flow directions.

Differences were also observed between seasons. In high-river-flow conditions (September), salinities on the mudflat did not exceed 5 PSU. In contrast, under low-flow conditions (March), the system was more strongly influenced by marine water (salinities up to 22 PSU; Figure 4i,j). Waves strongly influenced suspended sediment concentrations, with mean concentrations around two times greater in March than September (Fricke et al., in press).

Waves were almost always present, although wave heights varied. Under larger wave heights, wave breaking was widespread and likely contributed to alongshore flow in a manner similar to that observed on beaches. Wave heights decayed as waves propagated into the forest. In water depths of 1 m, models suggest that wave heights are expected to reduce by half by the time the waves propagate ~100 m into the forest. Although dissipation rates depend heavily on tree and root characteristics (Massel et al., 1999), these rates are similar to those recorded in other vegetated systems. For example, Horstman et al. (2014) reported maximum reduction rates of 44% at a location 100 m into a forest dominated by *Rhizophora mangle*, and Quartel et al. (2007) reported a 25%–50% reduction in wave height over 30 m in a forest of *Kandelia candel*. As in salt marsh systems, wave dissipation is most intense near the fringe (Jadhav et al., 2013).

Abruptly Changing Conditions on the Patch Scale

Even a casual comparison between measurements made on various days within and outside the forest reveals a clear influence of vegetation on turbulence levels. Figure 5a shows a snapshot of horizontal velocities on the mudflat, well outside the forest, from two vertically separated instruments (10 cm and 30 cm above the bed) with water depth 0.65 m. A few small wind waves ($H_s \sim 0.13$ m, periods ~ 2 s) are observed, and velocities from both heights are similar, with slightly smaller peak (negative)

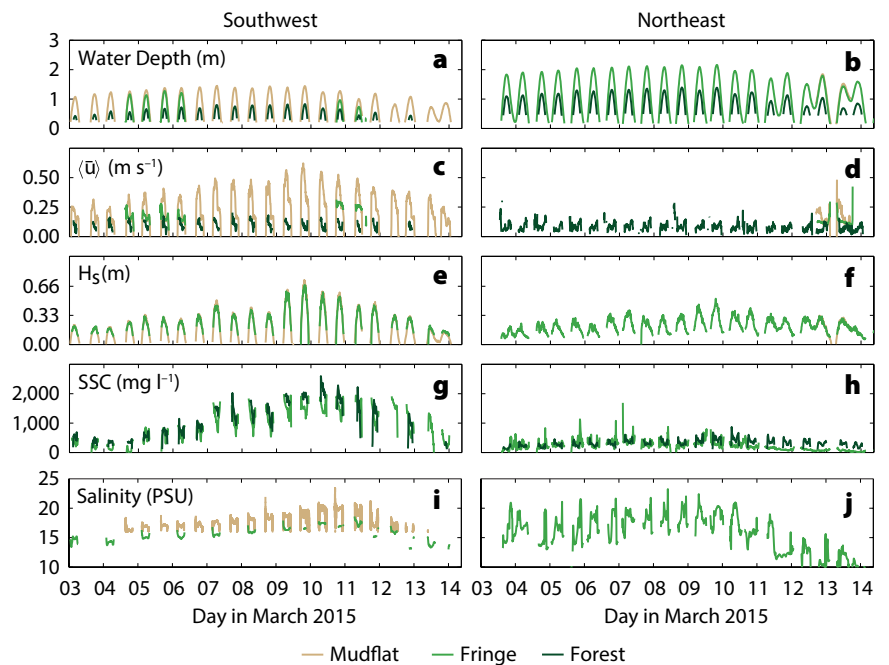


FIGURE 4. Graphs show (a,b) water depth, (c,d) depth-averaged and burst-averaged velocities, (e,f) significant wave height, (g,h) suspended sediment concentration (SSC), and (i,j) salinity from the southwest (left column) and northeast (right column) of Cu Lao Dung during the March experiment when more energetic wave conditions prevailed. Colors indicate instruments on mudflat (brown), fringe (light green), and forest (dark green). Note some instruments were part of the movable array, so records from a single location do not cover the full time. The velocity data were averaged over both a short vertical profile (~ 0.4 m near bed, light green) and the full water depth (dark green lines); mudflat velocities from (c) were single point measurements.

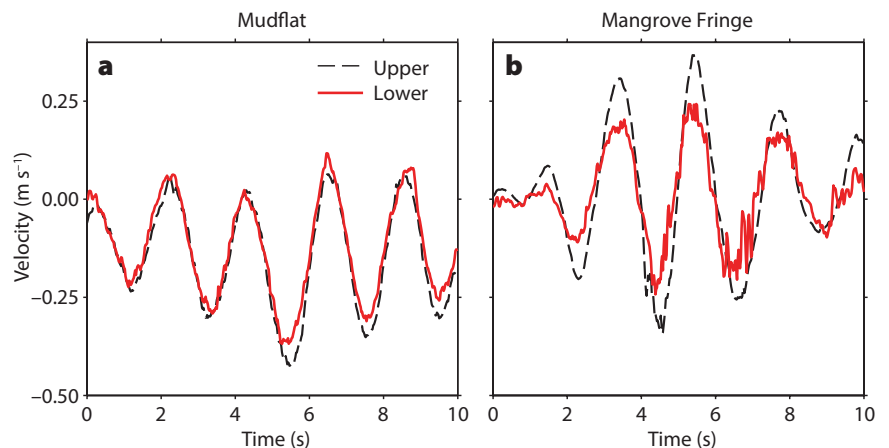


FIGURE 5. (a) Horizontal velocities from 30 m in front of the fringe on the mudflat at 0.1 m (red solid line) and 0.3 m (black dashed line) above the bed. Wave heights were 0.14 m and water depths 0.64 m. (b) Horizontal velocities from the fringe (20 m into trees) at 0.02 m above the bed (red solid line) within the pneumatophore canopy and 0.75 m above the bed and 0.15 m above the pneumatophore canopy (dashed black line). Wave heights were 0.28 m and water depths 1.46 m. Data were collected on (a) September 27, 2014, and (b) March 13, 2015.

velocities from the instrument closest to the bed. Figure 5b shows measurements in a water depth of 1.3 m from within and above the pneumatophore canopy (0.02 m and 0.75 m above bed) under similar wave conditions (wave height of 0.15 m). Although panels a and b do not show synoptic measurements, a comparison between the two nonetheless reveals some clear contrasts. As expected, in panel b, the velocities close to the bed are

more depth-attenuated than in panel a, simply owing to the larger vertical separation. However, inside the pneumatophore canopy, velocities are much more variable (see jagged red line) with high-frequency fluctuations superimposed on the wave flows. These high-frequency signals represent the turbulence generated as water flows back and forth past pneumatophores, creating small wakes and eddies. In contrast, much less

high-frequency turbulence is seen on the unvegetated mudflat (Figure 5a).

A sequence of profiles (Figure 6) for the dissipation rate of turbulent kinetic energy and suspended sediment concentrations (SSC) illustrates variability over different time scales (5 hrs, 2 hrs, 10 min, and 4 min). The estimates are from structure functions over three-minute windows, so turbulence from individual waves is not resolved; however, “hotspots” of turbulence are seen (e.g., from sequences of larger waves, wave breaking, and the interaction of multiple wakes). Turbulence is highly variable over all time scales (changing over four to five orders of magnitude throughout the experiment). In contrast, whereas the SSC show large changes over hours or each stage of the tidal cycle (panels b and d), over short time scales, values remain relatively consistent (panels f and h), emphasizing the integrative nature of these measurements. Turbulent dissipation rates, averaged over 10-minute bursts, often exceeded $10^{-4} \text{ W kg}^{-1}$, or even $10^{-3} \text{ W kg}^{-1}$. These values are much higher than in typical estuarine systems (Mullarney and Henderson, 2013) and are comparable to intensities measured near the bed in high-energy surf zones (Trowbridge and Elgar, 2001; Bryan et al., 2003; Feddersen, 2012). Synoptic measurements across three environments show that turbulence is elevated at the fringe relative to other locations (mudflat, forest).

Properties of the pneumatophore canopies, such as stem number and diameter, varied with both horizontal and vertical location. These parameters are particularly important to measure when defining relationships between turbulence levels and canopy density. A common contributor to horizontal variability was the grouping of pneumatophores into lines, with each line usually marking the presence of an underlying radial mangrove root. Variability in stem heights contributed to a fairly smooth decline of the key parameter $a(z)$ with height, from a maximum at the bed to zero at the top of the canopy. To account for vertical variability,

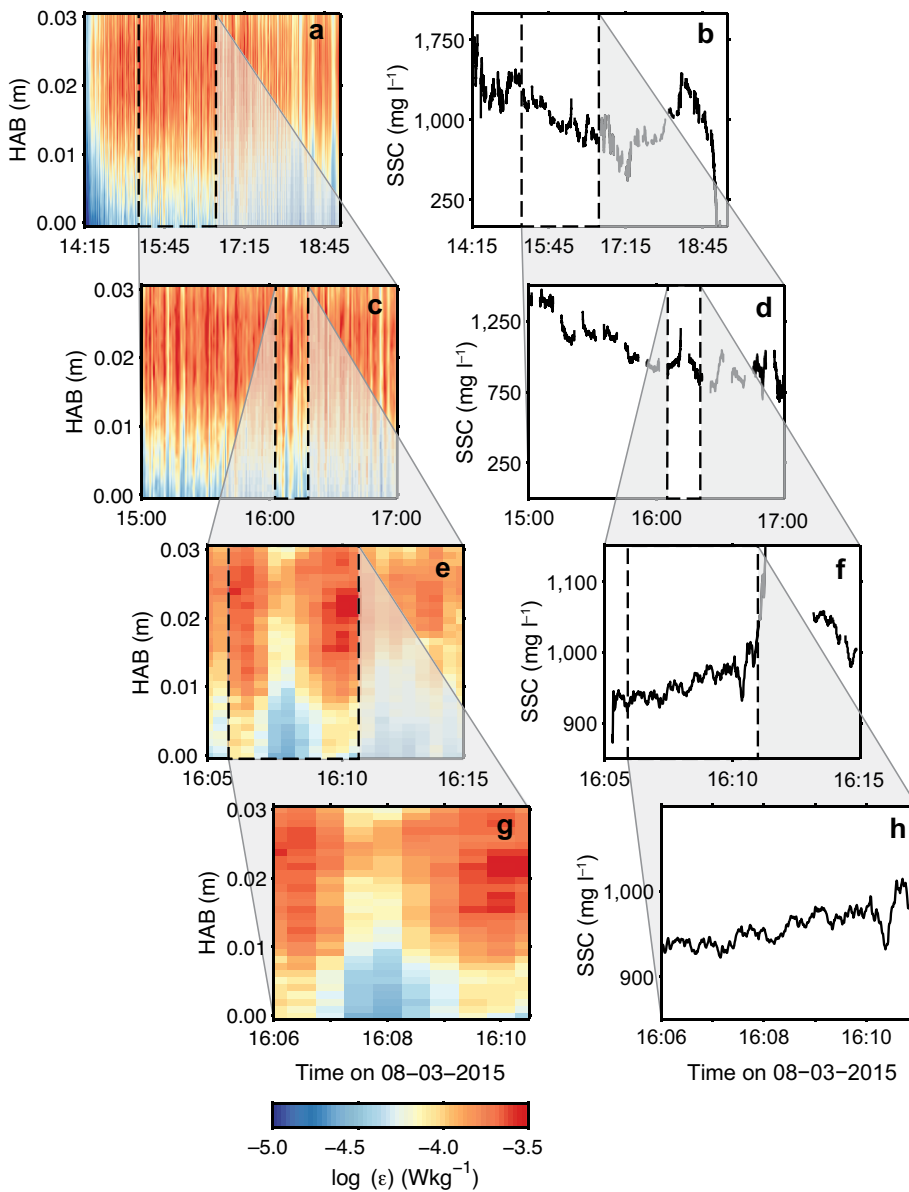


FIGURE 6. (a,c,e,g) Turbulence levels (dissipation rate of turbulent kinetic energy) within the pneumatophore canopy showing variability over multiple time scales. The cascade shows 5 hours, 2 hours, 10 minutes, and 4 minutes of data, with location of each subplot indicated by the shaded area between plots. (b,d,f,h) Variability of suspended sediment concentrations (SSC) is shown at the same time scales. SSC were measured at the mudflat-fringe transition, and turbulence was measured within the vegetation of the fringe. White spaces are data gaps between bursts. HAB is height above bed.

turbulence levels measured by each instrument were compared with canopy properties measured at that instrument elevation above the bed. To account for lateral variability, we aimed to identify the group of pneumatophores most directly responsible for inducing wakes (Figure 7a). To achieve this, mean flow directions over subsections of the tide (low, low-mid, mid-high, and high) were determined (Figure 7b). A 20 cm × 20 cm bounding box was then chosen to sample the region upstream of the Vectrino (Figure 7c,d), so that the instrument was on the downstream boundary of the box. After implementing this approach of selecting a small sampling box upstream of the instrument, turbulent dissipation was positively correlated with pneumatophore density measured by $a(z)$. The correlations were significant at the 90% confidence interval (p-value <0.1) between all four tidal subsections. In contrast, simply using a 1 m² quadrat centered on the instrument produced nonsignificant correlations for all tidal stages except the lowest (Norris et al., in press). This result suggests substantial spatial variability in turbulence levels throughout the pneumatophore canopy, and indicates a need to resolve submeter-scale variability when comparing turbulence with canopy geometry. Although we did not measure turbulence around tree trunks in the field, we have explored the relative role of tree trunks versus smaller pneumatophores in numerical modeling of the region. Although the tree canopies are visually the most dominant feature of the landscape, most of these branches and leaves do not contact the water, even at high tide, and therefore play a diminished role in shaping the currents. However, small-scale pneumatophores can substantially affect macroscale flows.

Turbulence is generated as water flows past vegetation stems, so it might be expected that the most dense vegetation patches at the forest fringe would be associated with the greatest turbulence levels. Roughly speaking, this expectation was supported by observations. Nevertheless,

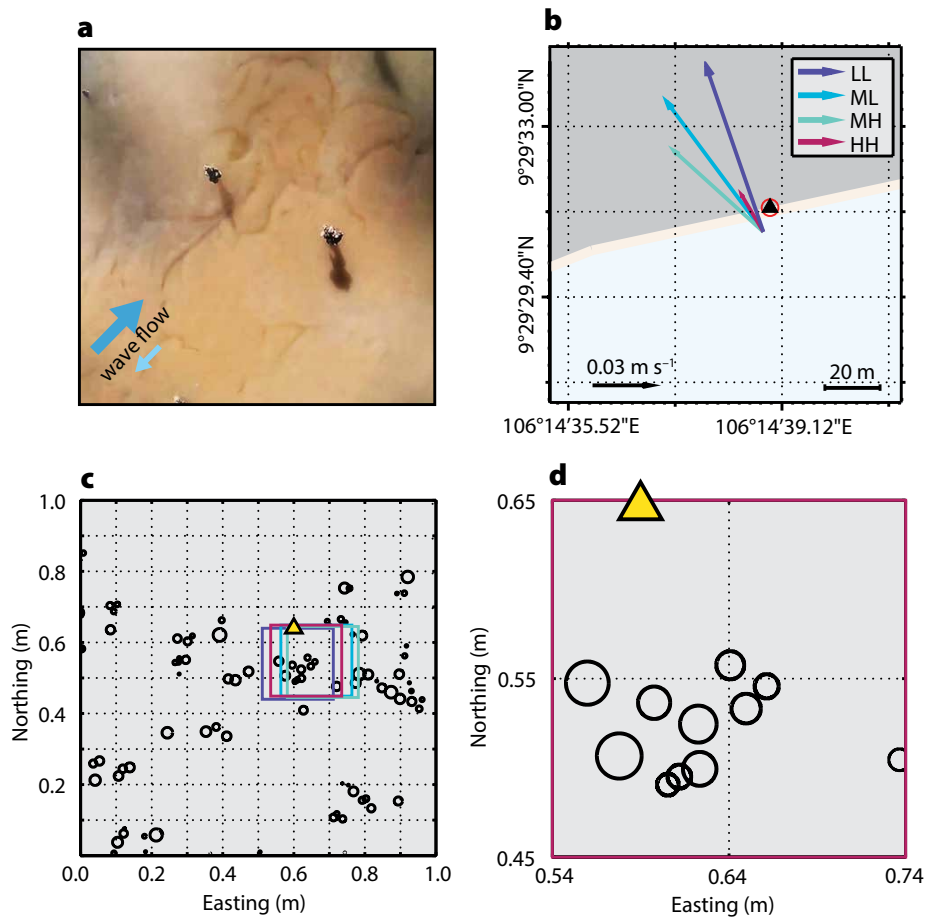


FIGURE 7. (a) Photograph from above showing wakes and eddies generated as water flows past pneumatophores. (b) Example of the changing mean flow directions from an instrument on the fringe with different stages of the tide indicated by colors: purple shows low tide (LL), light blue is low-to-mid tide (ML), green is mid-to-high tide (MH), and pink is high tide (HH). (c) Corresponding pneumatophore geometries in 1 m² quadrat from photogrammetric reconstruction. Black circles show basal diameters of pneumatophores, the yellow triangle indicates the location of a Vectrino Profiler, and colored boxes show (20 cm)² subsamples based on velocity directions at different stages of the tide and pneumatophores likely to cause wake turbulence. (d) (20 cm)² subsample from the height of the instrument for high tide.

it is interesting to note that in principle, turbulence is not always expected to increase with increasing vegetation density. In very high-density near-bed canopies, wave-frequency motions can become so sluggish that only limited turbulence is generated (this corresponds to the case shown in Figure 1a, if the vectors in this figure are taken to represent the magnitude of the oscillating flow; Henderson et al., in press). Consequently, there is a canopy density that yields maximal dissipation, with lower dissipation in both less-dense and more-dense canopies. This maximum occurs for order-one values of the dimensionless ratio, $\Lambda = T_w / (2\pi T_f)$, of the wave period (T_w) to the time scale for dissipation by canopy friction, T_f , (the frictional time scale

is the time that would be required for a reduction in velocity if forces other than friction suddenly ceased). The parameter Λ increases with vegetation density, and is a simple function of wave period and amplitude as well as vegetation geometry. For the observed Mekong Delta pneumatophore canopies, this Λ parameter was <1, and dissipation in the densest vegetation patches approached the theoretical maximum rates. This observation might have biological significance, because burial of pneumatophores by accumulating sediment can reduce mangrove health, or eventually cause death. Consequently, the observed pneumatophore canopies, which do not exceed the density for maximum dissipation, may have adaptive advantages in depositional

environments. While these results are suggestive, further work is required to develop quantitative models for pneumatophore effects on bed stress, sediment entrainment, and sediment mixing (variability in sediment size likely also plays a role; Nardin et al., 2016c).

TURBULENCE AND SEDIMENT TRANSPORT

After an energetic wave event, receding tides revealed fresh scour troughs around isolated pneumatophore stems on the tidal flats (Figure 8). At first glance, such erosion resembles a miniaturized version of the “local scour” often seen around artificial pilings (Sumer and Fredsøe, 2002). Scour often also extended

across entire patches of pneumatophores. Conversely, sandy sediment was deposited in gaps between lines of pneumatophores, causing locally raised regions of the seabed (Figure 8). The processes leading to this “global scour” extending across entire pneumatophore patches are not well established, but may differ from the simple secondary flow patterns known to influence the local scour around an isolated obstacle. Such patterns do not necessarily require lines of obstacles—similar erosion and deposition patterns were observed in laboratory experiments with a regular staggered array of rigid obstacles (Yager and Schmeckle, 2013).

The high-intensity turbulence we observed near the forest edge receives

energy from the dissipation of incident waves. Such intense turbulence could well have promoted winnowing of fine sediments and caused the observed erosion within pneumatophore patches. Interestingly, sediment on the mudflat was found to be relatively sandy within a few tens of meters of the forest edge, with significant grain-size fining over a short distance into the forest, especially in the low-energy September experiment (Figure 9). This distance over which bed composition changes (within 90 m in September and 150 m in March) is roughly consistent with the theoretical distance over which the waves are expected to lose their energy to turbulent dissipation (Henderson et al., in press). During

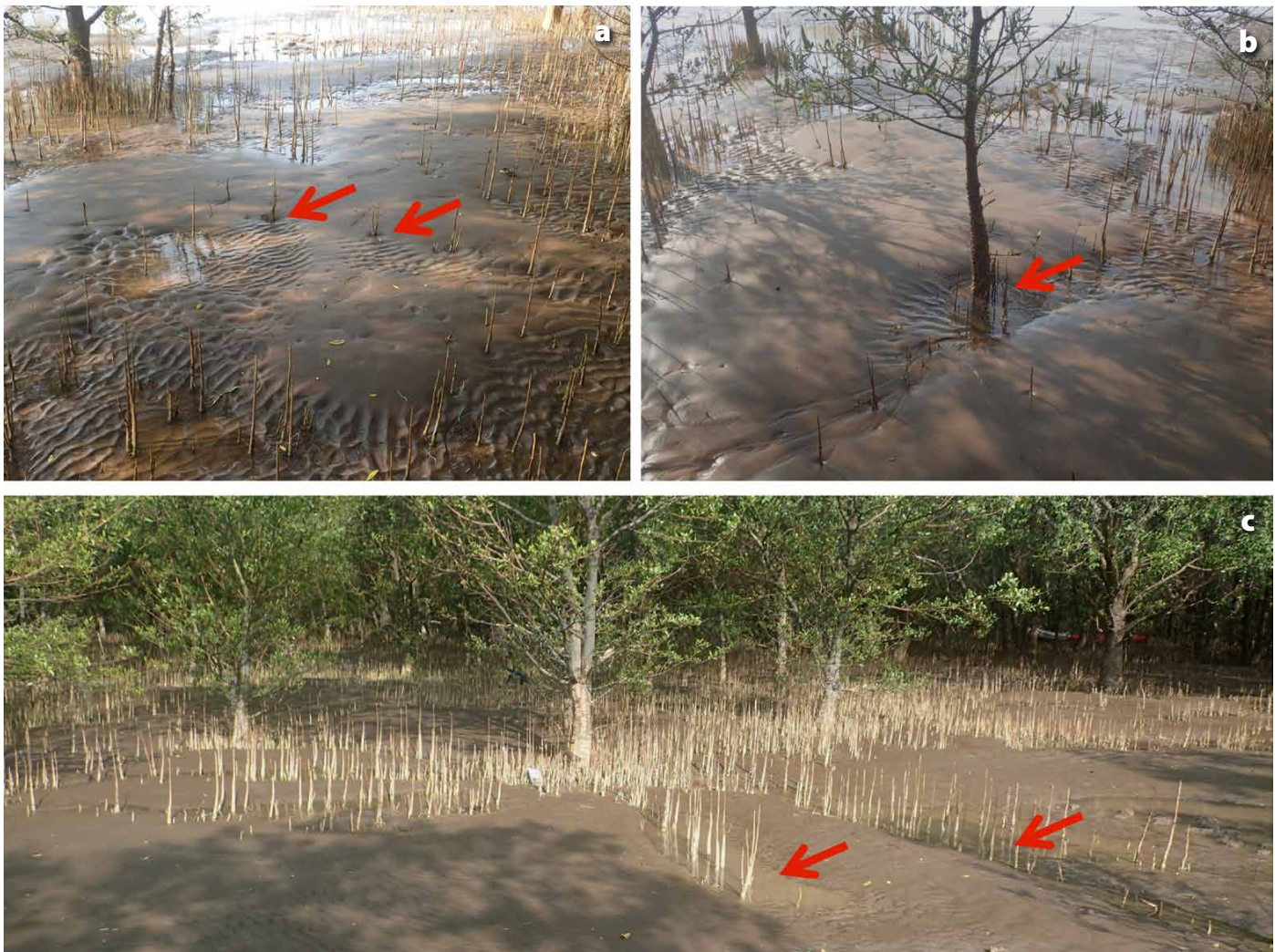


FIGURE 8. Photos taken in the mangrove fringe after an energetic wave event show (a) sand ripples and scour around individual pneumatophore roots, (b) scour around individual tree trunks, and (c) scour around patches of roots, with deposition of sand in the gaps between the lines of roots. Red arrows indicate a few examples of scour troughs.

September, much of the fining was associated with greater clay content of samples farther from the fringe. Such a pattern is consistent with winnowing of fine material from the bed near the highly turbulent forest edge. Some of this sediment may subsequently be transported onshore by flood-tide currents and be deposited during slack water at high tide, thereby accounting for the more clay-rich forest interior. This mechanism is consistent with the observed sediment fluxes: a larger and landward flux on the southwest side of the island, and a smaller and seaward flux on the low-energy and eroding northeast side (Figure 9).

Although our observations suggest that the distribution of sediments and small-scale turbulent processes may be linked, many questions still remain. For example, it is not clear whether the level of turbulence overall was the key parameter controlling sediment transport; intermittent vortices penetrating down to the bed and the influence of waves on the bed shear stress likely also played a role. Much additional work will be required before a testable model can be developed to predict how the distribution of turbulence controls sediment entrainment.

CONCLUSIONS AND CONUNDRUMS

The Fringe—A Hotspot for Change

The mangrove forest of Cu Lao Dung is a dynamic environment. When the seabed is exposed at low tide, in many ways the forest resembles its terrestrial counterpart, albeit with an unusual understory of pneumatophores. However, when inundated and subject to waves propagating and breaking through the trees, the environment is transformed into a system that has similarities not only with low-energy estuarine mangrove systems but also with surf zones, or structurally complex environments like coral reefs.

Our experiments reveal that the forest is characterized by complex and potentially interacting processes. In particular, our measurements show that the forest fringe is a dynamic and rapidly changing

area. Many key interrelated processes occur near the fringe (Figure 10). The fringe is the location of wave breaking and the most intense dissipation of energy. Pneumatophore densities tend to be greatest at the fringe, causing drag and abrupt flow rotation. Turbulence levels are also elevated at the fringe and, correspondingly, sediment within a thin strip (30 m and 90 m wide on southwest and northeast sides, respectively) along the fringe is much coarser. Hence, the amplification of turbulence near the forest fringe and the sheltering of inland regions may be linked: results suggest that fine sediments are likely transported from outside of the mangroves into the forest interior. The results raise questions about the existence of an ecogeomorphological feedback in which mangroves

grow roots in such a density and spacing as to promote scour near pneumatophores at the fringe to prevent burial, while simultaneously creating low-energy regions of sediment deposition farther inside the forest, thereby facilitating the progradation of the forest. Such patterns would be strongly mediated by the grain size and quantity of available sediments, which depend on the characteristics of the river and the shelf from which the sediment is sourced.

Overall, our results suggest that processes on small (centimeter) scales influence the large-scale dynamics across the entire forest. In particular, near the boundary between mudflat and mangrove forest, microscale turbulence may influence the balance of sediment erosion and deposition into and out of the

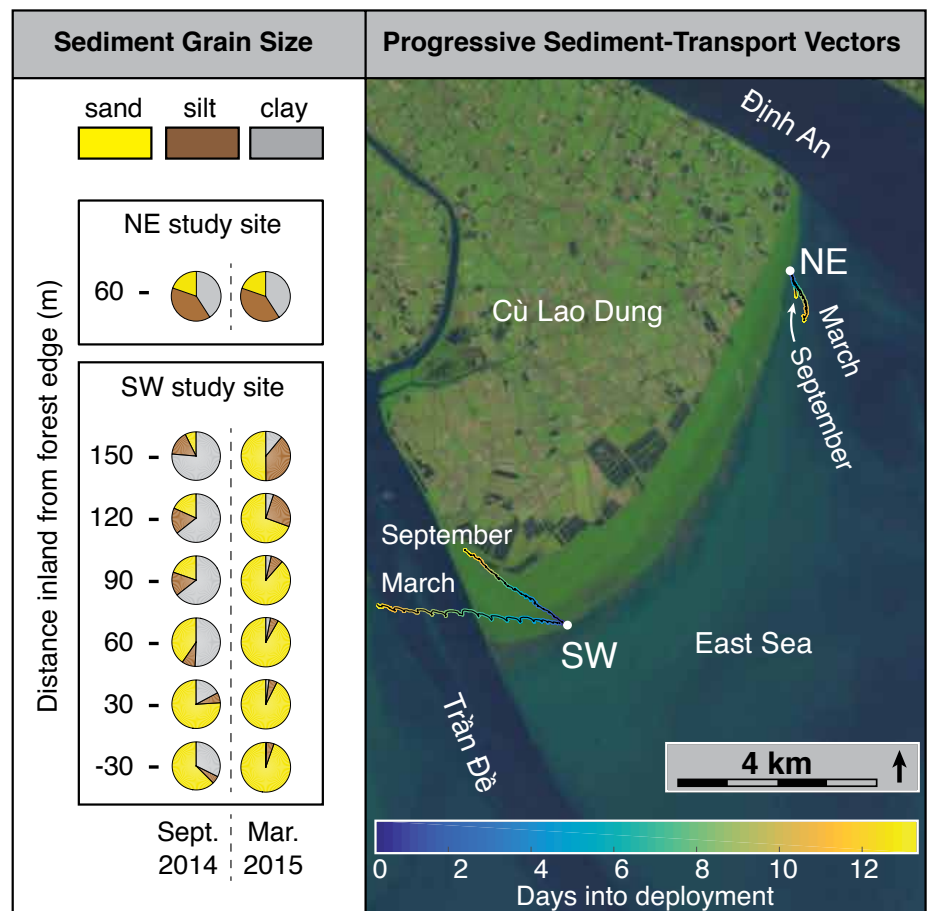


FIGURE 9. (left) Surface-sediment grain size at both sides of the forest and during the two different study periods. Pie charts show sand (yellow), silt (brown), and clay (gray) fractions in each sample. Increasing distances are measured into the forest from the forest edge. (right) Progressive vectors (colored by time) show the direction of sediment fluxes. Vectors are constructed by joining the sediment fluxes measured every 10 minutes in a tip-to-tail fashion. All four sets of vectors are the same scale.

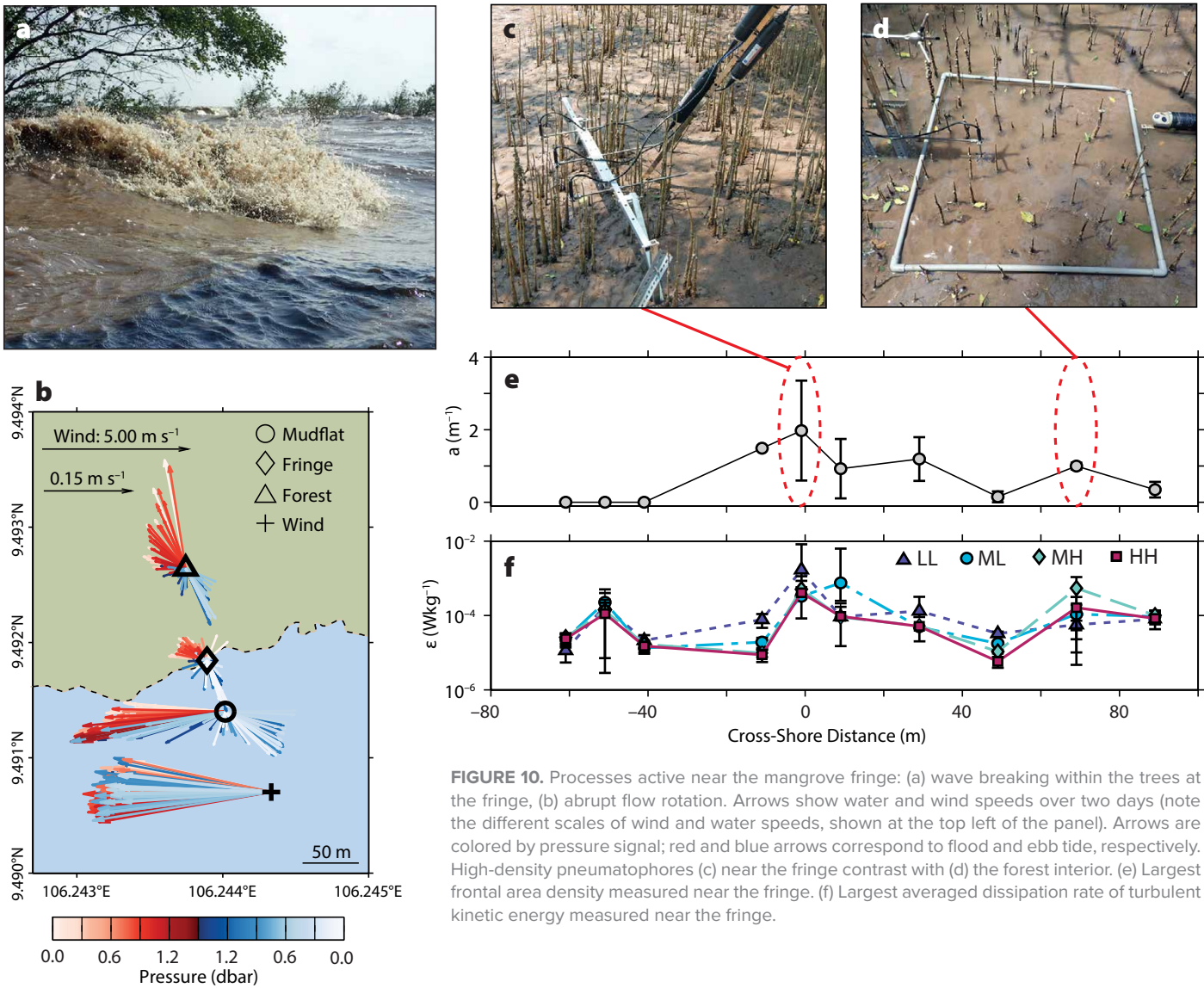


FIGURE 10. Processes active near the mangrove fringe: (a) wave breaking within the trees at the fringe, (b) abrupt flow rotation. Arrows show water and wind speeds over two days (note the different scales of wind and water speeds, shown at the top left of the panel). Arrows are colored by pressure signal; red and blue arrows correspond to flood and ebb tide, respectively. High-density pneumatophores (c) near the fringe contrast with (d) the forest interior. (e) Largest frontal area density measured near the fringe. (f) Largest averaged dissipation rate of turbulent kinetic energy measured near the fringe.

forest, and therefore play a role in the morphological evolution of the forest as a whole. Our observations suggest a need to develop quantitative models for bed stress, sediment suspension, and vertical mixing in highly turbulent forest fringe, as well as the relatively sheltered interior. Such models will be needed to predict the morphological resilience of these sensitive (often densely populated) environments to the increasingly imminent effects of sea level rise.

REFERENCES

- Allison, M.A., C.A. Nittrouer, A.S. Ogston, J.C. Mullarney, and T.T. Nguyen. 2017. Sedimentation and survival of the Mekong Delta: A case study of decreased sediment supply and accelerating rates of relative sea level rise. *Oceanography* 30(3):98–109, <https://doi.org/10.5670/oceanog.2017.318>.
- Anthony, E.J., G. Brunier, M. Besset, M. Goichot, P. Dussouillez, and V.L. Nguyen. 2015. Linking rapid erosion of the Mekong River delta to human activities. *Scientific Reports* 5, <https://doi.org/10.1038/srep14745>.
- Bear, J. 1979. *Hydraulics of Groundwater*. Dover, New York, 567 pp.
- Bouma, T.J., L.A. van Duren, S. Temmerman, T. Claverie, A. Blanco-Garcia, T. Ysebaert, and P.M.J. Herman. 2007. Spatial flow and sedimentation patterns within patches of epibenthic structures: Combining field, flume and modelling experiments. *Continental Shelf Research* 27:1020–1045, <https://doi.org/10.1016/j.csr.2005.12.019>.
- Bryan, K.R., K. Black, and R. Gorman. 2003. Spectral estimates of dissipation rate within and near the surf zone. *Journal of Physical Oceanography* 33:979–993, [https://doi.org/10.1175/1520-0485\(2003\)033<0979:SEODRW>2.0.CO;2](https://doi.org/10.1175/1520-0485(2003)033<0979:SEODRW>2.0.CO;2).
- Bryan, K.R., W. Nardin, J.C. Mullarney, and S. Fagherazzi. In press. The role of cross-shore tidal dynamics in controlling intertidal sediment exchange in mangroves in Cù Lao Dung, Vietnam. *Continental Shelf Research*, <https://doi.org/10.1016/j.csr.2017.06.014>.
- Bullock, E.L., S. Fagherazzi, W. Nardin, P. Vo-Luong, P. Nguyen, and C.E. Woodcock. In press. Temporal patterns in species zonation in a mangrove forest in the Mekong Delta, Vietnam, using a time series of Landsat imagery. *Continental Shelf Research*, <https://doi.org/10.1016/j.csr.2017.07.007>.
- Chen, Y., Y. Li, T. Cai, C. Thompson, and Y. Li. 2016. A comparison of biohydrodynamic interaction within mangrove and saltmarsh boundaries. *Earth Surface Processes and Landforms* 41:1967–1979, <https://doi.org/10.1002/esp.3964>.
- Coco, G., Z. Zhou, B. van Maanen, M. Olabarrieta, R. Tinoco, and I. Townend. 2013. Morphodynamics of tidal networks: Advances and challenges. *Marine Geology* 346:1–16, <https://doi.org/10.1016/j.margeo.2013.08.005>.
- Darby, S.E., C.R. Hackney, D.R. Parsons, J.L. Best, A.P. Nicholas, and R. Aalto. 2016. Fluvial sediment supply to a mega-delta reduced by shifting tropical-cyclone activity. *Nature* 539:276–279, <https://doi.org/10.1038/nature19809>.
- Fagherazzi, S., K.R. Bryan, and W. Nardin. 2017. Buried alive or washed away: The challenging life of mangroves in the Mekong Delta. *Oceanography* 30(3):48–59, <https://doi.org/10.5670/oceanog.2017.313>.
- Fagherazzi, S., M.L. Kirwan, S.M. Mudd, G.R. Guntenspergen, S. Temmerman, A. D'Alpaos, J. van de Koppel, J.M. Rybczyk, E. Reyes, C. Craft, and J. Clough. 2012. Numerical models of salt marsh evolution: Ecological, geomorphic, and climatic factors. *Reviews of Geophysics* 50, <https://doi.org/10.1029/2011RG000359>.

- Fedderson, F. 2012. Observations of the surf-zone turbulent dissipation rate. *Journal of Physical Oceanography* 42:386–399, <https://doi.org/10.1175/JPO-D-11-082.1>.
- Fricke, A.T., C.A. Nittrouer, A.S. Ogston, and H.P. Vo-Luong. In press. Asymmetric progradation of a coastal mangrove forest controlled by combined fluvial and marine influence, Cù Lao Dung, Vietnam. *Continental Shelf Research*, <https://doi.org/10.1016/j.csr.2017.07.012>.
- Henderson, S.M., B.K. Norris, J.C. Mullarney, and K.R. Bryan. In press. Wave-frequency flows within a near-bed vegetation canopy. *Continental Shelf Research*, <https://doi.org/10.1016/j.csr.2017.06.003>.
- Hong, P.N., and H.T. San. 1993. *Mangroves of Vietnam*. Vol. 7 of the International Union for Conservation of Nature and Natural Resources Wetlands Programme, 173 pp.
- Horstman, E.M., C.M. Dohmen-Janssen, T.J. Bouma, and S.J.M.H. Hulscher. 2015. Tidal-scale flow routing and sedimentation in mangrove forests: Combining field data and numerical modelling. *Geomorphology* 228:244–262, <https://doi.org/10.1016/j.geomorph.2014.08.011>.
- Horstman, E.M., C.M. Dohmen-Janssen, and S.J.M.H. Hulscher. 2013. Flow routing in mangrove forests: A field study in Trang province, Thailand. *Continental Shelf Research* 71:52–67, <https://doi.org/10.1016/j.csr.2013.10.002>.
- Horstman, E.M., C.M. Dohmen-Janssen, P.M.F. Narra, N.J.F. van den Berg, M. Siemerink, and S.J.M.H. Hulscher. 2014. Wave attenuation in mangroves: A quantitative approach to field observations. *Coastal Engineering* 94:47–62, <https://doi.org/10.1016/j.coastaleng.2014.08.005>.
- Jadhav, R.S., Q. Chen, and J.M. Smith. 2013. Spectral distribution of wave energy dissipation by salt marsh vegetation. *Coastal Engineering* 77:99–107, <https://doi.org/10.1016/j.coastaleng.2013.02.013>.
- Lanckriet, T., and J.A. Puleo. 2013. Near-bed turbulence dissipation measurements in the inner surf and swash zone. *Journal of Geophysical Research* 118:6,634–6,647, <https://doi.org/10.1002/2013JC009251>.
- Le Bouteiller, C., and J.G. Venditti. 2015. Sediment transport and shear stress partitioning in a vegetated flow. *Water Resources Research* 51:2,901–2,922, <https://doi.org/10.1002/2014WR015825>.
- Liénard, J., K. Lynn, N. Strigul, B.K. Norris, D. Gatzliolis, J.C. Mullarney, K.R. Bryan, and S.M. Henderson. 2016. Efficient three-dimensional reconstruction of aquatic vegetation geometry: Estimating morphological parameters influencing hydrodynamic drag. *Estuarine, Coastal and Shelf Science* 178:77–85, <https://doi.org/10.1016/j.ecss.2016.05.011>.
- Liu, J.P., D.J. DeMaster, T.T. Nguyen, Y. Saito, V.L. Nguyen, T.K.O. Ta, and X. Li. 2017. Stratigraphic formation of the Mekong River Delta and its recent shoreline changes. *Oceanography* 30(3):72–83, <https://doi.org/10.5670/oceanog.2017.316>.
- MacDonald, I.T., and J.C. Mullarney. 2015. A novel “FlocDrifter” platform for observing flocculation and turbulence processes in a Lagrangian frame of reference. *Journal of Atmospheric and Oceanic Technology* 32:547–561, <https://doi.org/10.1175/JTECH-D-14-00106.1>.
- Massel, S., K. Furukawa, and R. Brinkman. 1999. Surface wave propagation in mangrove forests. *Fluid Dynamics Research* 24:219–249, [https://doi.org/10.1016/S0169-5983\(98\)00024-0](https://doi.org/10.1016/S0169-5983(98)00024-0).
- Mazda, Y., E. Wolanski, B. King, A. Sase, D. Ohtsuka, and M. Magi. 1997. Drag force due to vegetation in mangrove swamps. *Mangroves and Salt Marshes* 1:193–199, <https://doi.org/10.1023/A:1009949411068>.
- Mullarney, J.C., and S.M. Henderson. 2013. A novel drifter designed for use with a mounted acoustic Doppler current profiler in shallow environments. *Limnology and Oceanography: Methods* 11:438–449, <https://doi.org/10.4319/lom.2013.11.438>.
- Mullarney, J.C., and S.M. Henderson. In press. Flows within marine vegetation canopies. In *Advances in Coastal Hydraulics*. V. Panchang, and J. Kaihatu, eds, World Scientific.
- Mullarney, J.C., S.M. Henderson, J.A.H. Reynolds, B.K. Norris, and K.R. Bryan. In press. Spatially varying drag within a wave-exposed mangrove forest and on the adjacent tidal flat. *Continental Shelf Research*, <https://doi.org/10.1016/j.csr.2017.06.019>.
- Nardin, W., and D.A. Edmonds. 2014. Optimum vegetation height and density for inorganic sedimentation in deltaic marshes. *Nature Geoscience* 7:722–726, <https://doi.org/10.1038/NGEO2233>.
- Nardin, W., D.A. Edmonds, and S. Fagherazzi. 2016a. Influence of vegetation on spatial patterns of sediment deposition in deltaic islands during flood. *Advances in Water Resources* 93:236–248, <https://doi.org/10.1016/j.advwatres.2016.01.001>.
- Nardin, W., S. Locatelli, V. Pasquarella, M.C. Rulli, C.E. Woodcock, and S. Fagherazzi. 2016b. Dynamics of a fringe mangrove forest detected by Landsat images in the Mekong River delta, Vietnam. *Earth Surface Processes and Landforms* 41:2,024–2,037, <https://doi.org/10.1002/esp.3968>.
- Nardin, W., C.E. Woodcock, and S. Fagherazzi. 2016c. Bottom sediments affect *Sonneratia* mangrove forests in the prograding Mekong Delta, Vietnam. *Estuarine, Coastal and Shelf Science* 177:60–70, <https://doi.org/10.1016/j.ecss.2016.04.019>.
- Nepf, H.M. 2012a. Flow and transport in regions with aquatic vegetation. *Annual Review of Fluid Mechanics* 44:123–142, <https://doi.org/10.1146/annurev-fluid-120710-101048>.
- Nepf, H.M. 2012b. Hydrodynamics of vegetated channels. *Journal of Hydraulic Research* 50:262–279, <https://doi.org/10.1080/00221686.2012.696559>.
- Nittrouer, C.A., J.C. Mullarney, M.A. Allison, and A.S. Ogston. 2017. Introduction to the special issue on sedimentary processes building a tropical delta yesterday, today, and tomorrow: The Mekong System. *Oceanography* 30(3):10–21, <https://doi.org/10.5670/oceanog.2017.310>.
- Norris, B.K., J.C. Mullarney, K.R. Bryan, and S.M. Henderson. In press. The effect of pneumatophore density on turbulence: A field study in a *Sonneratia*-dominated mangrove forest, Vietnam. *Continental Shelf Research*, <https://doi.org/10.1016/j.csr.2017.06.002>.
- Nowacki, D.J., A.S. Ogston, C.A. Nittrouer, A.T. Fricke, and P.D.T. Van. 2015. Sediment dynamics in the lower Mekong River: Transition from tidal river to estuary. *Journal of Geophysical Research* 120:6,363–6,383, <https://doi.org/10.1002/2015JC010754>.
- Pratolongo, P.D., G.M.E. Perillo, and M.C. Piccolo. 2010. Combined effects of waves and plants on a mud deposition event at a mudflat-saltmarsh edge in the Bahia Blanca estuary. *Estuarine, Coastal and Shelf Science* 87:207–212, <https://doi.org/10.1016/j.ecss.2009.09.024>.
- Quartel, S., A. Kroon, P.G.E.F. Augustinus, P. Van Santen, and N.H. Tri. 2007. Wave attenuation in coastal mangroves in the Red River Delta, Vietnam. *Journal of Asian Earth Sciences* 29:576–584, <https://doi.org/10.1016/j.jseaes.2006.05.008>.
- Sumer, B., and J. Fredsøe. 2002. *The Mechanics of Scour in the Marine Environment*. Advanced Series on Ocean Engineering, vol. 17, World Scientific, 552 pp.
- Syvitki, J.P.M., A.J. Kettner, I. Overeem, E.W.H. Hutton, M.T. Hannon, G.R. Brakenridge, J. Day, C. Vörösmarty, Y. Saito, L. Giosan, and R.J. Nicholls. 2009. Sinking deltas due to human activities. *Nature Geoscience* 2:681–686, <https://doi.org/10.1038/NGEO629>.
- Thorpe, S. 2005. *The Turbulent Ocean*. Cambridge University Press, 484 pp.
- Tinoco, R.O., and G. Coco. 2016. A laboratory study on sediment resuspension within arrays of rigid cylinders. *Advances in Water Resources* 92:1–9, <https://doi.org/10.1016/j.advwatres.2016.04.003>.
- Trowbridge, J., and S. Elgar. 2001. Turbulence measurements in the surf zone. *Journal of Physical Oceanography* 31:2,403–2,417, [https://doi.org/10.1175/1520-0485\(2001\)031<2403:TMITSZ>2.0.CO;2](https://doi.org/10.1175/1520-0485(2001)031<2403:TMITSZ>2.0.CO;2).
- van Maanen, B., G. Coco, and K.R. Bryan. 2015. On the ecogeomorphological feedbacks that control tidal channel network evolution in a dynamic mangrove setting. *Proceedings of the Royal Society A* 471, <https://doi.org/10.1098/rspa.2015.0115>.
- Wiles, P.J., T.P. Rippeth, J.H. Simpson, and P.J. Hendricks. 2006. A novel technique for measuring the rate of turbulent dissipation in the marine environment. *Geophysical Research Letters* 33, L21608, <https://doi.org/10.1029/2006GL027050>.
- Yager, E.M., and M.W. Schmeckle. 2013. The influence of vegetation on turbulence and bed load transport. *Journal of Geophysical Research* 118:1,585–1,601, <https://doi.org/10.1002/jgrf.20085>.

ACKNOWLEDGMENTS

We thank the Office of Naval Research (ONR) Global and the Office of Naval Research (USA) for funding (grant numbers N62909-14-1-N028 to JM and KB, N00014-14-10112 to SH, and N00014-12-1-0181, N00014-13-1-0075, N00014-13-1-0781, N00014-15-1-2014, N0014-15-1-2011, N0014-13-1-0127, which supported AF and DC), Andrea Ogston and Chuck Nittrouer from the University of Washington, H.P. Võ Lương, Xuan Tien Nguyen Vinh, and Hoang Phong Nguyen from the VNU University of Science (Ho Chi Minh City), and Rich Nguyen from ONR for their immense help in planning, organizing, and implementing the challenging logistics of the experiments and for assistance in the field. Thanks also to Sergio Fagherazzi and William Nardin from Boston University for assistance in the field.

AUTHORS

Julia C. Mullarney (julia.mullarney@waikato.ac.nz) is Senior Lecturer, School of Science, University of Waikato, New Zealand. **Stephen M. Henderson** is Associate Professor, School of the Environment, Washington State University, Vancouver, WA, USA. **Benjamin K. Norris** is a graduate student in the School of Science, University of Waikato, New Zealand. **Karin R. Bryan** is Associate Professor, School of Science, University of Waikato, New Zealand. **Aaron T. Fricke** is Postdoctoral Research Fellow, School of Oceanography, University of Washington, Seattle, WA, USA. **Dean R. Sandwell** is Technical Officer, School of Science, University of Waikato, New Zealand. **Daniel P. Culling** is a graduate student in the School of Science and Engineering, Tulane University, New Orleans, LA, USA.

ARTICLE CITATION

Mullarney, J.C., S.M. Henderson, B.K. Norris, K.R. Bryan, A.T. Fricke, D.R. Sandwell, and D.P. Culling. 2017. A question of scale: How turbulence around aerial roots shapes the seabed morphology in mangrove forests of the Mekong Delta. *Oceanography* 30(3):34–47, <https://doi.org/10.5670/oceanog.2017.312>.